DINAME 2023 - Proceedings of the XIX International Symposium on Dynamic Problems of Mechanics,
A.S. De Paula, A.T. Fabro and M.R. Machado (Editors), ABCM.
Pirenópolis, Go, Brazil, February 26th to March 3rd, 2023

A Multi-Physical Modeling Approach to ”Puffing” in Mechanical Face Seals

M. Gani[1], **W. Steeval**[1], **and I. F. Santos**[1]

[1] Technical University of Denmark, 2800 Kongens Lyngby

Abstract: In this work, a transient model of mechanical face seals in two-phase flow is presented and used to study ”puffing” phenomena. The model is one-dimensional, axisymmetric, and uses a multi-physical approach to describe the transient two-phase flow. This includes the equations of motion to describe the transient seal opening, a finite-volume implementation of the Reynolds and Energy equations, and a finite-element model of transient heat conduction in the seal rings, which has a dominating effect on seal performance. Transition between liquid and vapor phases is described using a thermodynamic saturation model based on the IAPWS-97 standard. This yields a system of Non-Linear Differential-Algebraic Equations (DAE), which is solved numerically in time. The model is validated for a steady-state case and then applied to study the transient behavior of mechanical face seals. The results of a simulation demonstrate damped ”puffing” oscillations which provide some qualitative insights into this type of behavior.

Keywords: mechanical face seal, phase-change, puffing, numerical simulation

NOMENCLATURE

CV	Control Volume
FD	Finite Difference
FE	Finite Element
FV	Finite Volume
$()_E$	Eastern node
$()_e$	Eastern face
$()_j$	Number of fx. CV or node
$()_P$	Centre node
$()_r$	Radial direction
$()_W$	Western node
$()_w$	Western face
$()_z$	Axial direction
$()_{theta}$	Tangential direction
$[()]$	Matrix
$\frac{D()}{Dt}$	$\frac{\partial()}{\partial t} + u_r\frac{\partial()}{\partial r} + u_\theta\frac{\partial()}{\partial \theta} + u_z\frac{\partial()}{\partial z}$
$\ddot{()}$	$\frac{\partial^2}{\partial t^2}$
Δ	Difference
$\dot{()}$	$\frac{\partial}{\partial t}$
$\{()\}$	Vector
∇	Divergence

$[K]$	Global heat conduction matrix
$[M]$	DAE mass matrix
$[M]$	Global mass matrix
$[R_q]$	Global heat flux linking matrix
$\dot{m}$	Mass flux
μ	Dynamic viscosity
$\{q\}$	Global heat flux vector
$\{R_h\}$	Global boundary convection vector
$\{y\}$	DAE state vector
ω	Rotational velocity
ϕ	Shearing work
ρ	Density
θ	Tangential Coordinate
A	Area
$A_{CV r\theta}$	CV surface area in the r-θ-plane
B	Balance ratio
$C_{P,D}$	Seal ring specific heat
F_C	Hydrostatic closing force
F_O	Opening force

F_s	Spring force
F_{res}	Resulting force
g	Gravitational acceleration
h	Film height
i	Specific enthalpy
k	Thermal conductivity coefficient
m_D	Seal ring mass
n_r	Number of radial nodes ($n_CV = n_r - 1$
n_z	Number of axial nodes in each seal ring
p	Pressure
q	Heat flux between fluid film and seal ring
r	Radial Coordinate
T	Temperature
t	Time
u	Velocity
V	Volume
z	Axial Coordinate

INTRODUCTION

Mechanical face seals are used to reduce leakage in rotating machinery by restricting flow in the radial direction in a pressurized environment, preventing it from escaping. This is accomplished via two concentric rings, a rotating ring mounted on the shaft and a stationary ring mounted on the housing. The two rings are pressed together tightly during operation, forming a thin interface between them, and creating resistance against the leakage flow in the radial direction. For the seal to function, a lubricating film must be formed between the seal surfaces, resulting in some amount of leakage. Under ideal circumstances, the film is sufficiently thin to maintain a tolerable amount of leakage while also sufficiently thick to ensure proper lubrication of the seal surfaces. As an example, a Grundfoss pump seal is illustrated in Fig. 1(a).

For water-lubricated seals operating with high fluid temperatures, part of the lubricating fluid may vaporize causing two-phase flow conditions. This causes a drastic change in the operating conditions of the seal that can lead to seal failure. Considering that most large and small-scale processes of modern society are dependent on water to function (energy production, transportation, agriculture, daily life, etc.), estimates suggest that water pumps consume up to 15% of the world's electricity (Abelin 2006, Augustyn 2012). Furthermore, studies have shown that 30-50% of water pump failure and repair costs are attributed to seal failure (Grundfos 2009). As such, mechanical face seals are an important area of research in the industry of rotating machinery. The focus of this work is the dynamic behavior of mechanical face seals and the phenomena of "puffing". Early experimental studies of mechanical face seals found evidence of unstable dynamic behavior related to oscillations induced by partial vaporization of the fluid film (Orcutt, 1969, Lymer and Greenshield, 1968, Lymer, 1973). The cyclic vaporization and condensation of the fluid film causing the seal to undergo unstable axial oscillations were termed "puffing" and have been a significant area of interest since. Later theoretical studies using semi-analytical discrete boiling models (DBM) were used to further study stability in seals and linked film thickness, pressure, and vaporization to unstable behavior in seals (Birchak and Hughes, 1997, Hughes, Winowich, and Birchak, 1978). Further studies suggested that puffing and seal stability may be related to the shape of the load versus film thickness curve and seal taper (Lebeck and Chiou, 1982). The conditions for stability were later studied using a dynamic two-phase flow model, showing that a converging seal gap generally has a stabilizing effect on seals operating in two-phase flow (Salant and Blasbalg, 1991 and 1995). Using more advanced continuous boiling models (CBM) it was shown that seal temperature may decrease with increased load due to vaporization. This model was also used to study stable and unstable zones of operation for seals in two-phase flow and how they are affected by the seal balance ratio (Migout, Brunetière, and Tournerie, 2015). Using a monolithic approach and implementation of saturation curves, the stability conditions for mechanical face seals in two-phase flow were studied using a steady-state multi-physics seal model, highlighting the conditions for puffing (Gani et al. 2022). The work presented in this paper expands upon this multi-physics model with the transient flow, heat transfer, and seal motions. This transient multi-physics two-phase flow seal model is used to simulate the dynamic behavior of mechanical seals in two-phase flow, showing a seal operating with unstable oscillations caused by vaporization or "puffing".

MATHEMATICAL MODEL

The mechanical face seal is described by an unsteady multi-physical model consisting of several equations, divided into a fluid domain (1), solid domain (2), and the interface between the two domains (3), as highlighted in Fig. 1(b). Finally, the fluid film thickness is described by axial motions of the rotating ring, given by the equations of motion from standard dynamics. Further elaboration on the equations can be found in (Gani et al. 2022).

1. Fluid domain
    - Flow and energy in the fluid film are described the continuity equation and a simplified Energy equation using the finite-volume method (FV).
    - Phase-transformation is described by a saturation function derived from the IAPWS-IF97 standard.
2. Interface
    - Heat transfer between the fluid film and seal rings is described by a semi-analytical wall heat flux equation.
3. Solid domain
    - Heat conduction in the seal rings is described by a finite-element model (FE).

The primary assumptions used in deriving these equations include: thin film, axisymmetry, constant properties across the fluid film (density, viscosity, pressure, no flow in the axial direction) and two-phase regions are a homogeneous mixture of liquid and vapor. These assumptions greatly simplify the equations used to describe the physical problem.

Combined, the equations form a system of differential-algebraic equations (DAE) that are solved using a solver for stiff differential equations. In this case, the ode15s solver from MatLab is used but any appropriate method for DAEs can be used.

Fluid Properties

As the fluid transitions from liquid to gas, the fluid properties change dramatically. By using CBM instead of DBM a model for gas and liquid mixtures is needed. The partly evaporated fluid is modeled as a homogeneous mixture, meaning that the mixture of gas and liquid is seen as a pseudo fluid with properties equal-weighted averages of the mixture fluids.

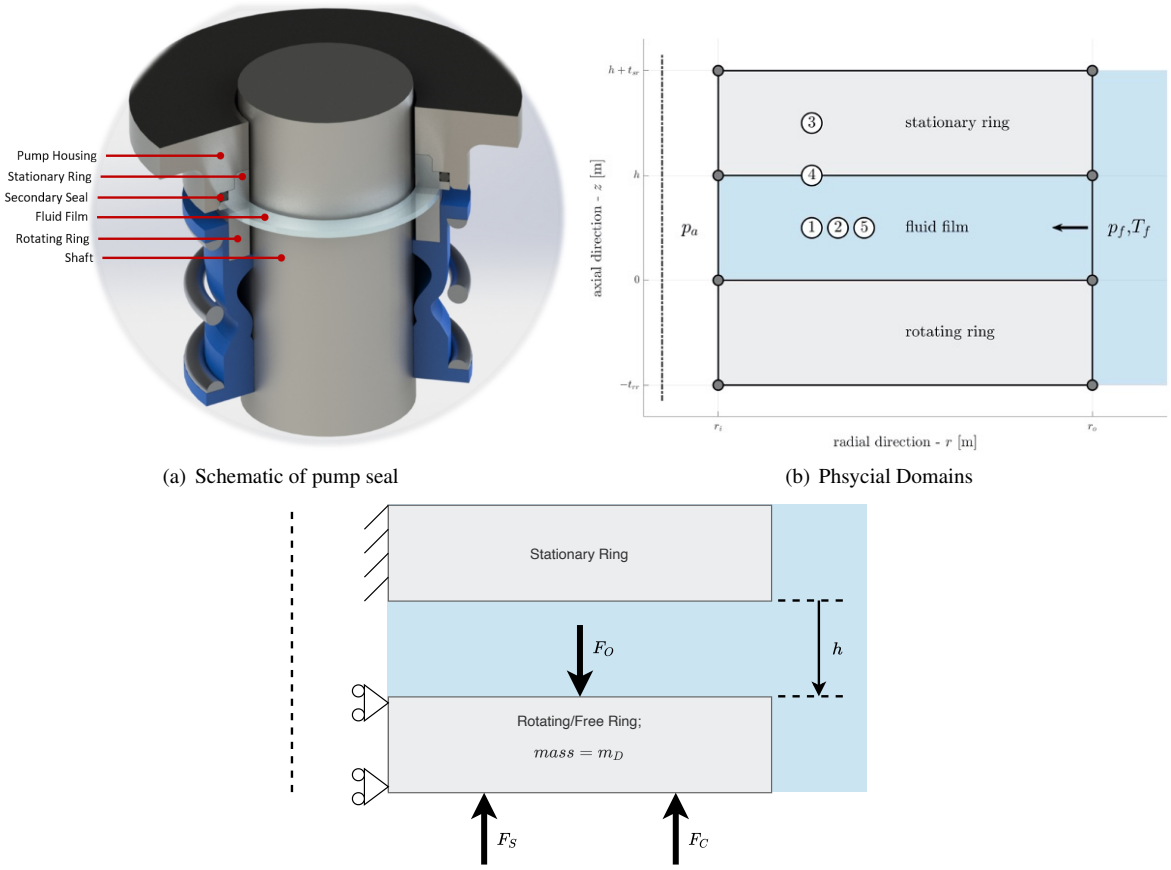

(a) Schematic of pump seal

(b) Phsycial Domains

(c) Free Body Diagram of the free/rotating ring

Figure 1 – Illustration of the seal and physical domains

As a weighing factor, the vapor mass fraction (quality) is used.

$$\lambda = \begin{cases} \lambda = 1 & \text{for}, i > i_{v,Sat} \\ \lambda = \dfrac{i - i_{l,Sat}}{i_{v,Sat} - i_{l,Sat}} & \text{for}, i_{l,Sat} < i < i_{v,Sat} \\ \lambda = 0 & \text{for}, i < i_{l,Sat} \end{cases} \tag{1}$$

The fluid properties are averaged with the following weighting, where $_v$ indicates vapor phase property and $_l$ indicates liquid phase property (Saadat and Flint, 1996).

$$\begin{aligned} \frac{1}{\rho(p,T)} &= \frac{\lambda}{\rho_v(p,T)} + \frac{(1-\lambda)}{\rho_l(T)} \\ \frac{1}{\mu(p,T)} &= \frac{\lambda}{\mu_v(p,T)} + \frac{(1-\lambda)}{\mu_l(T)} \end{aligned} \tag{2}$$

Ideal Gas Law is used to estimate the density of the vapor phase.

Governing Equations

The motion of the rotating seal ring is modeled as a 1 DOF mass system illustrated in Fig. 1(c). The rotating ring is free to move axially and has the following equation of motion, where F_O is the opening force caused by the pressure profile between the seal rings. F_C is the hydrostatic closing force caused by pressures acting on the outside of the seal rings. F_S is the closing force caused by springs if present. The spring force may both consist of a static pretension and/or stiffness.

$$m_D \ddot{h} = F_{res} = F_O - (F_C + F_s) \tag{3}$$

The fluid domain is modeled using the conservation of mass and momentum. Applying simplifying assumptions, and inserting momentum conservation into mass conservation yields Eq. 12. The Finite-Volume (FV) method is used to handle the nonlinear equations. Gradients are approximated by a Finite-Difference (FD) scheme.

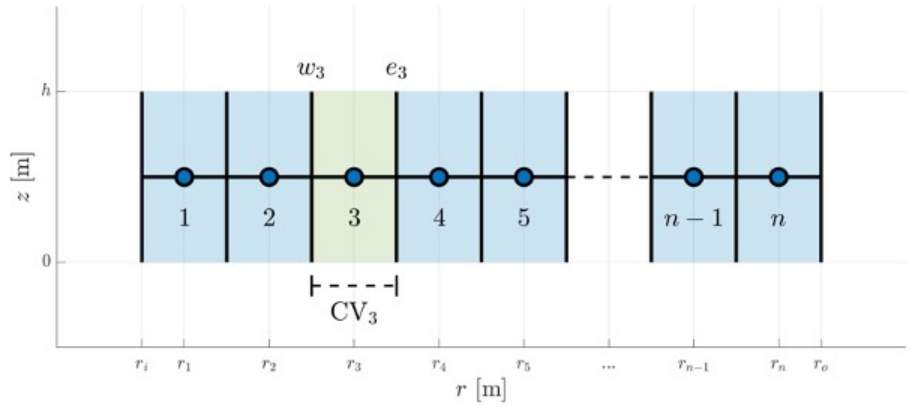

Figure 2 – FV mesh

$$\rho \frac{D\{u\}}{Dt} = -\nabla p + \rho\{g\} + \mu\nabla^2\{u\} \tag{4}$$

$$0 = \frac{\partial}{\partial t}\int_V \rho dV + \int_S \rho\{u\}\cdot\{n\}dA \tag{5}$$

With an order of scale analysis, it can be seen that inertial terms are insignificant in the radial direction and that shearing forces are only significant in the r-z plane. Furthermore, the assumptions eliminate pressure gradients except in the radial direction, along with body forces. These reductions result in a Poiseuille flow in the radial direction, and a Couette flow in the tangential direction.

$$0 = -\frac{\partial p}{\partial r} + \mu\frac{\partial^2 u_r}{\partial z^2} \qquad\qquad 0 = \frac{\partial^2 u_\theta}{\partial z^2} \tag{6}$$

Considering the boundary conditions, one obtains the expressions for the velocity components.

$$u_r(r,z) = \frac{1}{2\mu}\frac{\partial p}{\partial r}\left(z^2 - hz\right) \qquad\qquad u_\theta(r,z) = \omega r\frac{z}{h} \tag{7}$$

Inserting the velocity components into the mass conservation results in a governing equation for the fluid flow.

$$0 = 2\pi r\Delta r\frac{\partial\left(h_P\rho_P\right)}{\partial t} + \left(-2\pi r\rho\frac{h^3}{6\mu}\frac{\partial p}{\partial r}\right)\Bigg|_w^e \tag{8}$$

At a given CV the state of the fluid is given by 2 independent variables - pressure and enthalpy. The enthalpy is known from energy conservation on the fluid film.

$$\frac{D(\rho i)}{Dt} = \frac{Dp}{Dt} + \nabla\cdot(k\nabla\cdot T) + \phi + \tilde{q} \tag{9}$$

Using the simplifying assumptions and an order of scale analysis reduces the equation to,

$$\frac{\partial\rho i}{\partial t} + u_r\frac{\partial\rho i}{\partial r} = \frac{\partial p}{\partial t} + u_r\frac{\partial p}{\partial r} + \phi + \tilde{q} \tag{10}$$

The heat transfer through the seal rings is modeled as solid heat transfer.

$$\rho C_P\frac{\partial T}{\partial t} - k\left(\frac{\partial^2 T}{\partial r^2} + \frac{1}{r}\frac{\partial T}{\partial r} + \frac{\partial^2 T}{\partial z^2}\right) = 0 \tag{11}$$

Saturations tables are used to determine the quality (vapor mass fraction) of the fluid, in each CV. The saturation tables are precomputed using the IAPWS-97 standard.
The heat transfer between the solid domain and the fluid domain is assumed to be dominated by a parabolic temperature distribution in the fluid illustrated in Fig. 3.

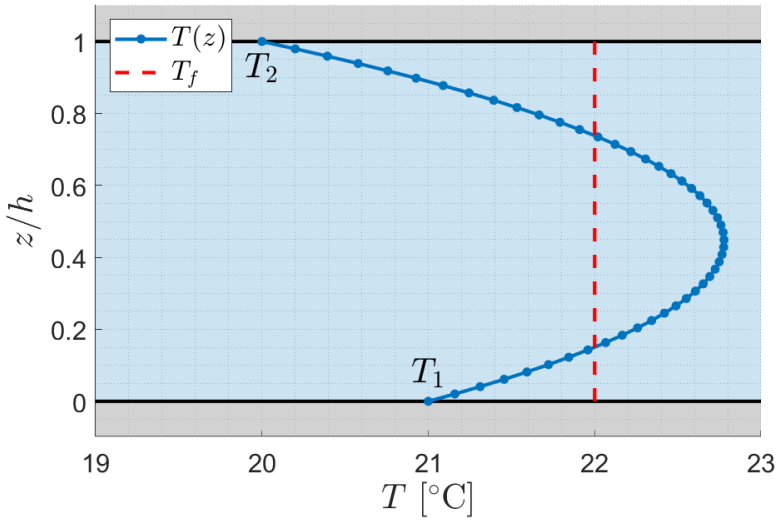

Figure 3 – Parabolic temperature variation in the fluid

NUMERICAL IMPLEMENTATION

The FV method is used to model the fluid domain, where gradients are approximated using a FD scheme. The FV method is already implemented in the fluid flow equation (8). Using FD on the fluid domain yields the following approximation for pressure gradients.

$$\left.\frac{\partial p}{\partial r}\right|_{e_3} \approx \frac{p_4 - p_3}{r_4 - r_3} \tag{12}$$

Applying FV to the energy equation yields,

$$2\pi r\Delta r\frac{\partial\left(h_P\rho_P i_P\right)}{\partial t} + (\dot{m}i)\Big|_w^e = 2\pi r\Delta r\frac{\partial\left(h_P p_P\right)}{\partial t} + (Qp)\Big|_w^e + 2\pi r\Delta r\left(h_P\phi + q\right) \tag{13}$$

The Finite Element (FE) is used to model the solid domain. Applying FE to the solid heat transfer equation, one obtains;

$$\{\dot{T}_i\} = [M]^{-1}\left(\frac{-[K]\{T_i\} + \{R_h\} + [R_q]\{q_i\}}{C_{P,D}}\right) \tag{14}$$

Applying the Finite Element and Finite Volume to the heat transfer equation, yields,

$$\{q_1\}\Big(\{T_f\},\{T_1\},\{T_2\}\Big) = \frac{k_1}{h}\left(6\{T_f\} - [M_T]\left(2\{T_2\} + 4\{T_1\}\right)\right) \tag{15}$$

$$\{q_2\}\Big(\{T_f\},\{T_1\},\{T_2\}\Big) = \frac{k_2}{h}\left(6\{T_f\} - [M_T]\left(4\{T_2\} + 2\{T_1\}\right)\right) \tag{16}$$

$$\{q\}\Big(\{T_f\},\{T_1\},\{T_2\}\Big) = \{q_1\} + \{q_2\} \tag{17}$$

where,

$$[M_T] = \frac{1}{2}\begin{bmatrix} 1 & 1 & 0 & \dots & 0 \\ 0 & 1 & 1 & \dots & 0 \\ \vdots & & \ddots & \ddots & \vdots \\ 0 & \dots & 0 & 1 & 1 \end{bmatrix} \tag{18}$$

The model is implemented as a system of differential and algebraic equations (DAE). The model is implemented in a manner compatible with MATLAB's ode15s solver. The implementation consists of a state vector and a time derivative of this state vector. A 'mass matrix' is used to indicate whether a row describes an algebraic or differential equation.

$$[M]\frac{\partial\{y\}}{\partial t} = f(t,\{y\}) \tag{19}$$

$$\{y\} = \begin{Bmatrix} h \\ \dot{h} \\ \{i\} \\ \{T_1\} \\ \{T_2\} \\ \{p\} \end{Bmatrix} \qquad \frac{\partial \{y\}}{\partial t} = \begin{Bmatrix} \dot{h} \\ \ddot{h} \\ \{\dot{i}\} \\ \{\dot{T}_1\} \\ \{\dot{T}_2\} \\ \{\dot{p}\} \end{Bmatrix} \qquad [M] = \begin{bmatrix} 1 & 0 & 0 & 0 & 0 & 0 \\ 0 & 1 & 0 & 0 & 0 & 0 \\ 0 & 0 & [I] & 0 & 0 & 0 \\ 0 & 0 & 0 & [I] & 0 & 0 \\ 0 & 0 & 0 & 0 & [I] & 0 \\ 0 & 0 & 0 & 0 & 0 & 0 \end{bmatrix} \tag{20}$$

Numerical Problems

Implementing the model with dimensional values result in an ill-conditioned problem. The difference in magnitude between pressure $\mathcal{O}(10^6)$ and fx. film height $\mathcal{O}(10^{-6})$ resulted in a stiff system matrix resulting in loss of numerical precision. To resolve this, the equations and variables were made non-dimensional.
Computation time was the second big obstacle. It was found that the method for evaluating heat transfer between fluid and rings caused a large stiffness in the system for small film heights. With this limitation, it was not practically possible to perform simulations below 1μm of minimum film thickness.

NUMERICAL RESULTS

Validation Case

Seal Parameters		**Value**	
Inner Radius	r_i	36.5125	mm
Outer Radius	r_o	42.8625	mm
Taper Angle	θ	0	rad
Axial Thickness	h_D	18	mm
Thermal Conductivity	κ	50	W/mK
Specific Heat Capacity	C	470	$\mathrm{J\,kg^{-1}}$
Density	ρ	1800	$\mathrm{kg\,m^{-3}}$
Number of Radial Nodes	n_r	151	
Number of Axial Nodes	n_r	10	
Operating Parameters		**Value**	
Pumped Fluid Temperature	T_F	207	°C
Pumped Fluid Pressure	p_F	2000	kPa
Atmospheric Pressure	p_{atm}	101	kPa
Rotational Velocity	ω	4000	RPM
Initial/Constant Film Height	h_0	1	µm

Table 1 – Parameters for the simulation

A study of subcooling and stability for seals in two-phase flow (Lau et al. 1990) was used for validating the modeling procedure and assumptions made in this work. This study was also compared to the steady-state results, i.e., disregarding time changes, obtained by Gani (2022). The parameters for the simulation are presented in Tab. 1 and the steady state fluid film pressure along the seal radius is depicted in Fig. 4. It is important to highlight that the steady state results for the pressure are obtained using the transient model until steady state results are reached, with the film height locked to a constant value. The results of the validation illustrate the pressure and boiling locus described by Lau. Despite a slight discrepancy in the location of the boiling point, the models are found to agree quite well. The fluid pressure is extremely sensitive to small changes in temperature, meaning minor differences in the model may lead to a slightly different temperature field.

Transient Case - Puffing

After validating the code under steady state conditions, the simulation of "puffing" is carried out using the transient model, and the results are shown in Figs. 5, 6, and 7. Once again the parameters of Tab. 1 are used except for the film height which is kept free to move with an initial film height of 1 µm. In Figure 5 the behavior of the fluid film height as well as the fluid film temperature depending on the time is depicted. It is seen that the film height increases from 1 µm to 30 µm from 0 until 0.08 seconds. The collar ring reaches an equilibrium position (height) to match the opening and closing forces generated by the fluid film, which starts changing cyclically its phase from liquid (low values of film height) to vapor (high values of film height) and vice versa. When the seal opens due to the change in film forces from vaporization, the leakage flow increases, reducing the sealing efficiency. After 0.08 seconds, the seal collar ring begins oscillating between a high and low film thickness, i.e., from ca. 4 µm to 15 µm as part of the fluid film vaporizes and condenses. In the same figure, it is seen that the seal ring surface temperature also responds to these changes, corresponding to the

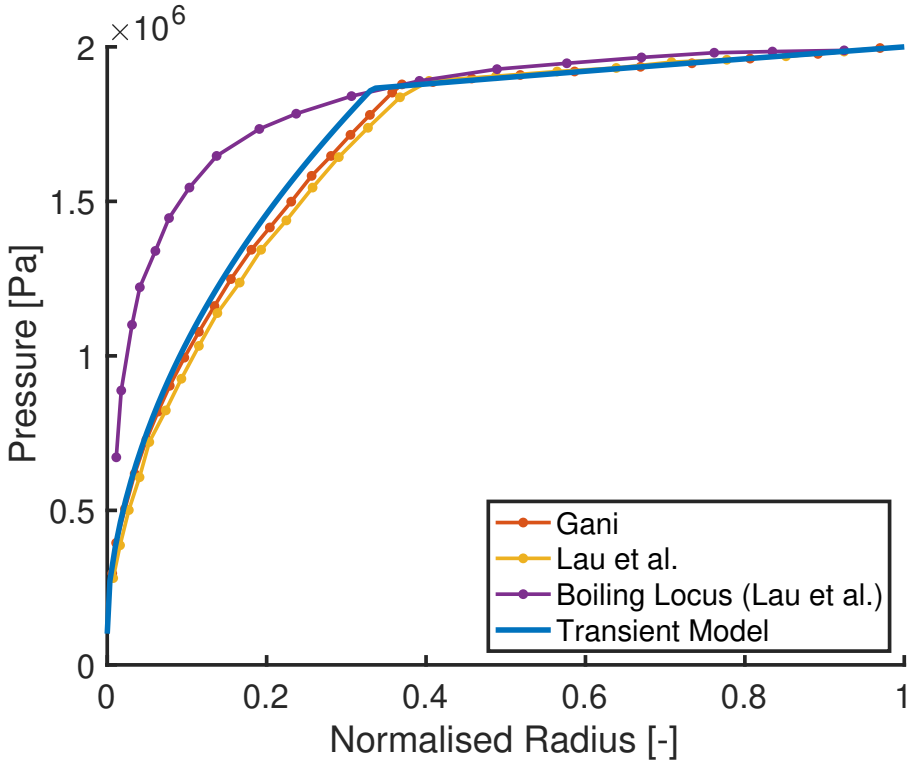

Figure 4 – Two-Phase flow pressure field validation results.

alternating state of the fluid film. From ca. 0.08 until 0.20 seconds the seal opens 6 times, leading to a "puffing" frequency of approx. 50 Hz, i.e., 6 oscillation / (0.20 – 0.08) seconds.

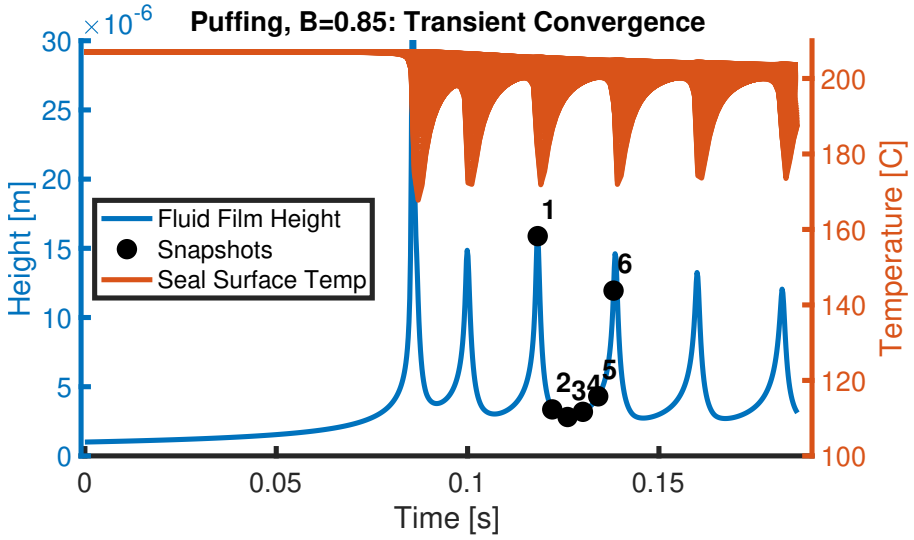

Figure 5 – Film height and seal surface temperature

In Fig. 6(a) it is seen that the boiling point moves with the same frequency, demonstrating the effect of cyclical vaporization and condensation. In the final two oscillations, a very interesting complex behavior of the boiling point is observed. Starting at a boiling point valley, the boiling point slowly moves towards the outer radius. Approximately halfway to the peak, the slope steepens. It then plateaus for approximately a quarter of the period after which it immediately drops to the valley and starts over. It is also seen that the boiling point seems to have a slight phase-shift compared to the film height (seen compared to the leakage rate). This behavior is exactly how "puffing" is described in a seal. In essence, every time the seal closes, energy in the form of heat is generated from viscous friction, causing more of the film to vaporize and release a "puff" of vapor as the seal opens again. The energy generated from viscous forces should end up balancing the energy dissipation, causing the oscillation to continue and keep opening the seal in a constant periodic fashion. The

pressure fields and vapor mass fraction at the peaks and valleys of the oscillation are shown in Fig. 6(b). At the peaks, the fluid partially vaporizes leading to a reduction in the pressure field and opening force (the opening force is defined by the area under the pressure curve). At the valley before popping open again a small section of the fluid is completely vaporized causing an increase in pressure and opening force. This is consistent with the "puffing" behavior observed in the other figures.

This evaporation pattern highlights the power of a CBM model. While the evaporation is very discrete at low film thicknesses (exemplified by the valley quality distribution in Fig. 6(b)), a large film thickness restricts the heat transfer between fluid and walls, resulting in wide continuous boiling resembling adiabatic evaporation.

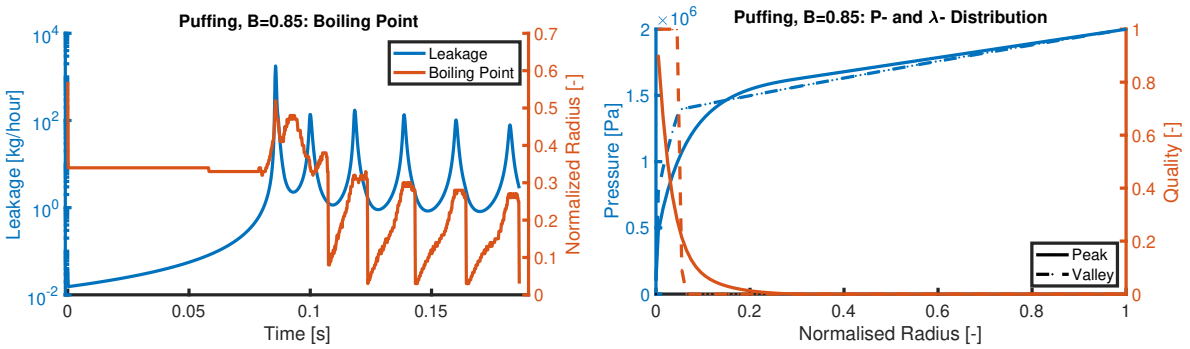

(a) Boiling Point (b) Pressure and quality distribution

Figure 6 – Time Periodic oscillation

Finally, Fig. 7 shows 6 snapshots of one puffing cycle. It is seen that at the peak (Snap 1) the film has a wide partial evaporation zone. Then as the film collapses (Snap 2) the film at the inner radius evaporates completely, raising the entire pressure profile. This causes downward deacceleration. Then in Snap 3-5, it is seen that the seal rings and fluid heat up. Simultaneously, the boiling point moves deeper into the seal. The seal now accelerates upwards due to high values of opening force. Finally, at the last step before the peak (snap 6) the evaporation zone begins to widen again, and the point with complete evaporation moves towards the inner radius.

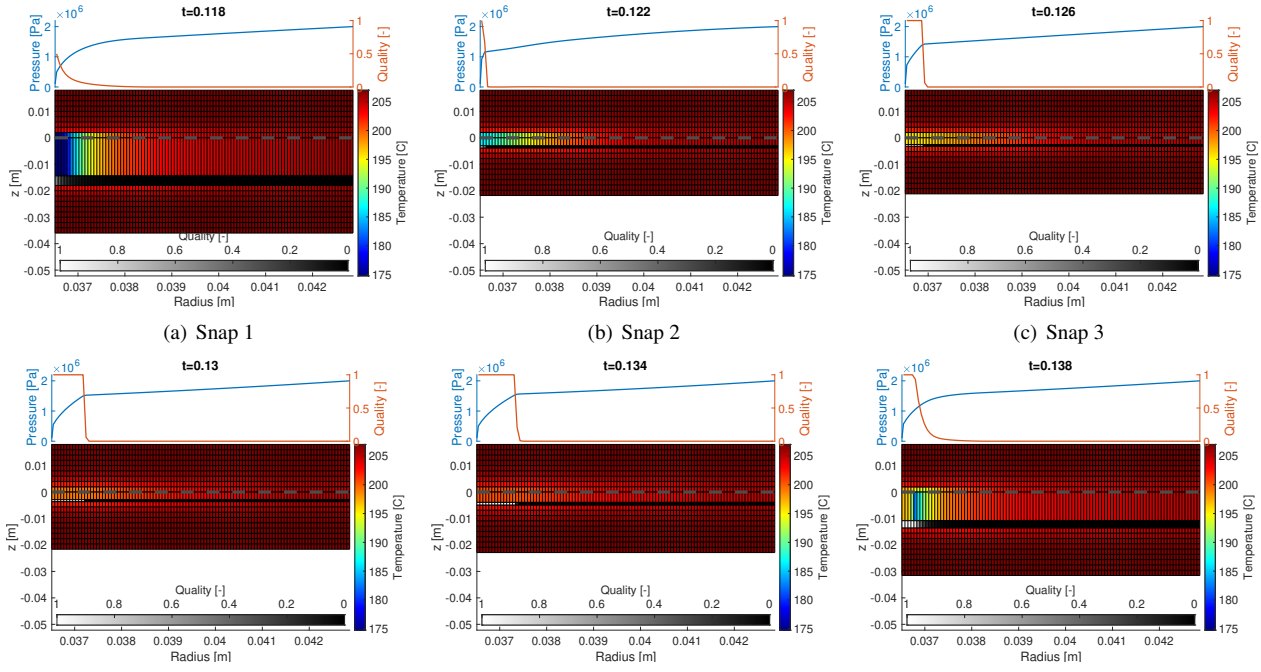

(a) Snap 1 (b) Snap 2 (c) Snap 3

(d) Snap 4 (e) Snap 5 (f) Snap 6

Figure 7 – Time Periodic oscillation

CONCLUSION

A transient multi-physics model of mechanical seals in two-phase flow was derived from the steady-state model by Gani et al. (2022). The mathematical model was implemented and validated for a steady-state case of two-phase flow originally presented by Lau et al. (1990). The transient model was found to be in good agreement with these results. A simulation of unstable dynamic seal behavior was then presented, illustrating "puffing". These results demonstrate a "puffing" cycle where the seal slowly heats up, after which it pops open. The seal then oscillates between a closed and open state. The axial oscillations of the film thickness are accompanied by a cyclical variation in both temperature and boiling radius. This explains how the seal releases a "puff" of water vapor and opens up, followed by a condensation of the vapor zone and decrease in opening forces, causing the seal to close again.

REFERENCES

Stefan M. Abelin. Improving pumping system performance: A sourcebook for industry, second edition, report, 2006. Golden, Colorado. https://digital.library.unt.edu/ark:/67531/ metadc891947/, University of North Texas Libraries, UNT Digital Library; accessed June 15, 2022).

T. Augustyn. Energy efficiency and savings in pumping systems - the holistic approach. 2012 Southern African Energy Efficiency Convention, Saeec 2012, page 6408587, 2012.

M. Birchak and W. F. Hughes. Simplified computer program for the analysis of phase change in liquid face seals, 1977. Prepared for NASA, Lewis Research Center.

D. A. Blasbalg and R. F Salant. Numerical study of two-phase mechanical seal stability. Tribology Transactions, 38(4):791–800, 1995.

M. Gani, I. F. Santos, M. Arghir, and H. Grann. Model validation of mechanical face seals in two-phase flow conditions. Tribology International, 167:107417, 2022.

Mechanical shaft seals for pumps, (2009. GRUNDFOS Management A/S).

W. F. Hughes, N. S. Winowich, M. J. Birchak, and W. C. Kennedy. Phase-change in liquid face seals. Journal of Lubrication Technology-transactions of the Asme, 100(1):74

S. Y. Lau, W. F. Hughes, P. Basu, P. A. Beatty, A simplified model for two phase face seal design, Tribology Transactions 33(3) (1990) 315–324

A. O. Lebeck and B. C. Chiou. Two-phase mechanical face seal operation: Experimental and theoretical observations, 1982. Available electronically from https://hdl.handle.net/1969.1/163703, accessed June, 2022.

A. Lymer. Mechanical seals. Tribology, 6(6):57–61, 1973.

A. Lymer and A. L. Greenshield. Thermal aspects of mechanical seals. Pumps, 24(7):209, 1968.

F. Migout, N. Brunetière, and B. Tournerie. Study of the fluid film vaporization in the interface of a mechanical face seal. Tribology International, 92:84–95, 2015.

F. K. Orcut. An investigation of the operation and failure of mechanical face seals. Journal of Lubrication Technology, 91(4):713–725, 1969.

R. F. Salant and D. A. Blasbalg. Dynamic behavior of 2-phase mechanical seals. Tribology Transactions, 34(1):122–136, 1991.

N. Saadat, W. L. Flint, Expressions for the viscosity of liquid/vapour mixtures : Predicted and measured pressure distributions in a hydro- static bearing, Institution of Mechanical Engineers, Part J: Journal of Engineering Tribology 210(1) (1996) 75–79